Molecular Therapy
Original Article

A Basic ApoE-Based Peptide Mediator to Deliver Proteins across the Blood-Brain Barrier: Long-Term Efficacy, Toxicity, and Mechanism

Yu Meng,[1,2,10] Jennifer A. Wiseman,[1,10] Yuliya Nemtsova,[1] Dirk F. Moore,[3] Jenieve Guevarra,[4] Kenneth Reuhl,[5] William A. Banks,[6,7] Richard Daneman,[8] David E. Sleat,[1,9] and Peter Lobel[1,9]

[1]Center for Advanced Biotechnology and Medicine, Rutgers, The State University of New Jersey, Piscataway, NJ 08854, USA; [2]Wenzhou-Kean University, Wenzhou, Zhejiang 32050, China; [3]Department of Biostatistics, School of Public Health, Rutgers, The State University of New Jersey, Piscataway, NJ 08854, USA; [4]Department of Pharmacology, Physiology, and Neuroscience, Rutgers New Jersey Medical School, Newark, NJ 07103, USA; [5]Department of Pharmacology and Toxicology, Rutgers, The State University of New Jersey, Piscataway, NJ 08854, USA; [6]Geriatrics Research Education and Clinical Center, Department of Medicine, Veterans Affairs Puget Sound Health Care System, Seattle, WA 98108, USA; [7]Division of Gerontology and Geriatric Medicine, University of Washington School of Medicine, Seattle, WA 98108, USA; [8]Departments of Pharmacology and Neuroscience, University of California, San Diego, CA 92093, USA; [9]Department of Biochemistry and Molecular Biology, Rutgers, The State University of New Jersey, Piscataway, NJ 08854, USA

We have investigated delivery of protein therapeutics from the bloodstream into the brain using a mouse model of late-infantile neuronal ceroid lipofuscinosis (LINCL), a lysosomal disease due to deficiencies in tripeptidyl peptidase 1 (TPP1). Supraphysiological levels of TPP1 are delivered to the mouse brain by acute intravenous injection when co-administered with K16ApoE, a peptide that in trans mediates passage across the blood-brain barrier (BBB). Chronic treatment of LINCL mice with TPP1 and K16ApoE extended the lifespan from 126 to >294 days, diminished pathology, and slowed locomotor dysfunction. K16ApoE enhanced uptake of a fixable biotin tracer by brain endothelial cells in a dose-dependent manner, suggesting that its mechanism involves stimulation of endocytosis. Pharmacokinetic experiments indicated that K16ApoE functions without disrupting the BBB, with minimal effects on overall clearance or uptake by the liver and kidney. K16ApoE has a narrow therapeutic index, with toxicity manifested as lethargy and/or death in mice. To address this, we evaluated variant peptides but found that efficacy and toxicity are associated, suggesting that desired and adverse effects are mechanistically related. Toxicity currently precludes direct clinical application of peptide-mediated delivery in its present form but it remains a useful approach to proof-of-principle studies for biologic therapies to the brain in animal models.

INTRODUCTION

Drug delivery is a critical challenge for the effective treatment of a broad range of neurological disorders including Alzheimer and Parkinson disease, traumatic brain injury, and cancer. Such disorders also include numerous hereditary neurodegenerative diseases such as lysosomal storage disorders (LSDs), which are rare individually but collectively represent a significant problem. Intravenous (i.v.) administration is a relatively non-invasive route of drug delivery and the extensive microvasculature of the brain potentially allows for widespread distribution. However, the blood-brain barrier (BBB) has proven to be a particularly difficult obstacle to the effective delivery of both large- and small-molecule therapeutics to the brain.[1,2]

We have recently conducted proof-of-principle experiments on a system that allows delivery of therapeutics from the bloodstream to the brain.[3] Our experiments focused on a mouse model[4] for late-infantile neuronal ceroid lipofuscinosis (LINCL), a neurodegenerative LSD of children caused by the loss of the 66-kDa lysosomal glycoprotein, tripeptidyl peptidase 1 (TPP1).[5] Restoration of TPP1 in the brain is required to cure the disease, and we have demonstrated that delivery via lumbar intrathecal injection can have significant therapeutic benefits.[6] However, little (<10% of wild-type levels with a 2-mg dose)[7] or negligible (with a 1-mg dose)[3] recombinant human TPP1 (rhTPP1) is delivered to the brain when it is administered i.v. to the LINCL mouse model and there is no effect on disease progression.[3] In contrast, when rhTPP1 is co-administered with K16ApoE, a 36-residue peptide[8] containing 16 lysines followed by a 20-amino-acid sequence from apolipoprotein E (ApoE), there is robust delivery of rhTPP1 throughout the brain. Initial studies using an acute-treatment regimen demonstrated beneficial effects in the LINCL mouse.[3] The K16ApoE delivery system has also been successfully used to deliver other proteins as well as small molecules to the brain.[3,8]

Received 12 December 2016; accepted 29 March 2017;
http://dx.doi.org/10.1016/j.ymthe.2017.03.037.

[10]These authors contributed equally to this work.

Correspondence: Peter Lobel, Center for Advanced Biotechnology and Medicine, Rutgers University, 679 Hoes Lane, Piscataway, NJ 08854, USA.
E-mail: lobel@cabm.rutgers.edu
Correspondence: David E. Sleat, Center for Advanced Biotechnology and Medicine, Rutgers University, 679 Hoes Lane, Piscataway, NJ 08854, USA.
E-mail: sleat@cabm.rutgers.edu

The mechanism by which K16ApoE mediates protein passage across the BBB remains unclear. Early work indicated that when highly basic peptides and proteins (e.g., protamine, polylysine, and polyarginine) are administered via carotid artery injection, they can promote transport of proteins across the BBB in the ipsilateral hemisphere.[9,10] However, polycation-mediated uptake is ineffective in the contralateral hemisphere or when administered via tail vein injection, and we have found that tail vein coadministration of protamine does not promote the uptake of rhTPP1 to the brain.[3] This is a key difference from K16ApoE, which promotes widespread uptake of rhTPP1 across the entire brain. Thus, K16ApoE has unique pharmacological properties that distinguish it from polycations. Polycations including polylysine are associated with toxicity in vivo and in vitro. Mechanisms underlying toxicity remain unclear (reviewed in Ballarín-González and Howard[11]) but may include the induction of necrotic and/or apoptotic cytotoxic pathways as a result of disruption of the plasma and/or internal membranes,[12,13] or interaction with serum proteins or erythrocytes resulting in aggregate formation (microthrombi) that may occlude microcapillaries within the lungs or other organs.[14,15]

Numerous cell penetrating peptides, including HIV-1 TAT, HSV-1 VP22, and *Drosophila* ANTP (reviewed in Bolhassani et al.[16]), have been described that have the potential to deliver covalently associated macromolecules into cells. The mechanisms of action appear varied and are not fully understood but in many, a positive charge appears important. One possibility is that these peptide sequences electrostatically interact with negatively charged glycosaminoglycans (GAGs) to bind and enter target cells. Utility in terms of promoting protein delivery across the BBB remains controversial.[17] It is worth noting that the delivery of TAT conjugates to cells is inhibited by polyanions such as heparin.[18]

While an efficient delivery route for proteins and other drugs across the BBB is an extremely exciting prospect that could potentially open novel avenues of treatment for numerous neurological diseases, the K16ApoE peptide mediator of brain targeting has a narrow therapeutic index and kills mice at high doses when administered i.v.[3] The aim of this study was to determine whether toxicity of K16ApoE would preclude its use in a chronic manner to treat the LINCL mouse and to further understand both its mechanism of action and adverse properties.

RESULTS

Chronic Peptide-Mediated i.v. Enzyme Replacement Therapy

Tpp1$^{-/-}$ mice were treated with weekly i.v. administration of 40 nmol (180 μg) K16ApoE and/or 17 nmol (1 mg) rhTPP1, initiating treatment at 6 weeks of age and continuing until the animals died or when they reached the investigator-specified endpoint of age 42 weeks. Treatment with K16ApoE and rhTPP1 significantly increased the lifespan of the *Tpp1*$^{-/-}$ mice, with a median survival of 247 days compared to 126, 137, or 116 days for historical untreated controls or controls that were treated with rhTPP1 alone or K16ApoE alone, respectively (Figure 1A). A number of animals administered K16ApoE alone died immediately or shortly after dosing, indicating that there was death due to acute toxicity of the peptide rather than disease progression. Thus, we also analyzed all treatment groups after censoring for infusion-related deaths (Figure 1B). After doing so, treatment with K16ApoE alone had no effect on survival, while median survival of the animals treated with rhTPP1 and K16ApoE together was increased to more than 294 days, the predetermined endpoint of the study. Note that more infusion-related deaths were observed in animals administered K16ApoE alone than K16ApoE with rhTPP1. While this might suggest that K16ApoE is more toxic in the absence of protein, we believe that this is not the case and that this difference is simply stochastic. For example, K16ApoE was equally toxic in dose-response studies conducted in the presence of either 0.12 or 1 mg rhTPP1.[3] In addition, 120 nmol K16ApoE was similarly toxic in the absence of co-administered protein, or with 3.2 mg rhTPP1 or 16 mg BSA (Table S1).

Gait analysis revealed that administration of rhTPP1 in the presence of K16ApoE ameliorated the decline of locomotor function in LINCL mice (Figures 1C and 1D). Western blot analysis of the major storage material in LINCL, subunit c of mitochondrial ATP synthase (SCMAS) (Figure 1E), revealed greatly diminished levels in the 42-week-old treated LINCL mice compared to untreated 17-week-old animals and approached that found in wild-type mice. At 17 weeks, SCMAS levels in LINCL mice treated with K16ApoE or rhTPP1 alone were similar to those of untreated animals, while levels in animals treated with rhTPP1 and K16ApoE together were again similar to wild-type mice (data not shown).

Brain Distribution of rhTPP1 Delivered by K16ApoE-Mediated Uptake

To determine the general distribution of rhTPP1 throughout the brain, we synthesized fluorescent rhTPP1 and administered it to wild-type mice by tail vein injection in the presence and absence of K16ApoE. Whole-slide imaging of sagittal sections revealed that in the absence of K16ApoE, there was strong staining in the choroid plexus as expected, but little or none of the rhTPP1 localized to the parenchyma of the brain (Figure 2). However, close examination did reveal punctate cytoplasmic localization of rhTPP1, which is consistent with delivery to the lysosome and/or other intracellular vesicles within the endothelial cells or capillaries and larger blood vessels (Figure 3). This indicates that in the absence of K16ApoE, rhTPP1 can be endocytosed by cells proximal to the bloodstream but there appears to be little or no transcytosis into adjacent neurons.

When administered in conjunction with K16ApoE, whole-slide imaging of sagittal and coronal brain sections indicates that the fluorescent rhTPP1 is widely distributed throughout the brain (Figures 2 and 4). While rhTPP1 fluorescence was detected most strongly around major blood vessels (see magnified insets of blood vessels in the cerebellum and midbrain, Figure 4), it was detected within the parenchyma, with lower levels in surface proximal regions and higher levels in the deeper regions of the brain. For example, delivery

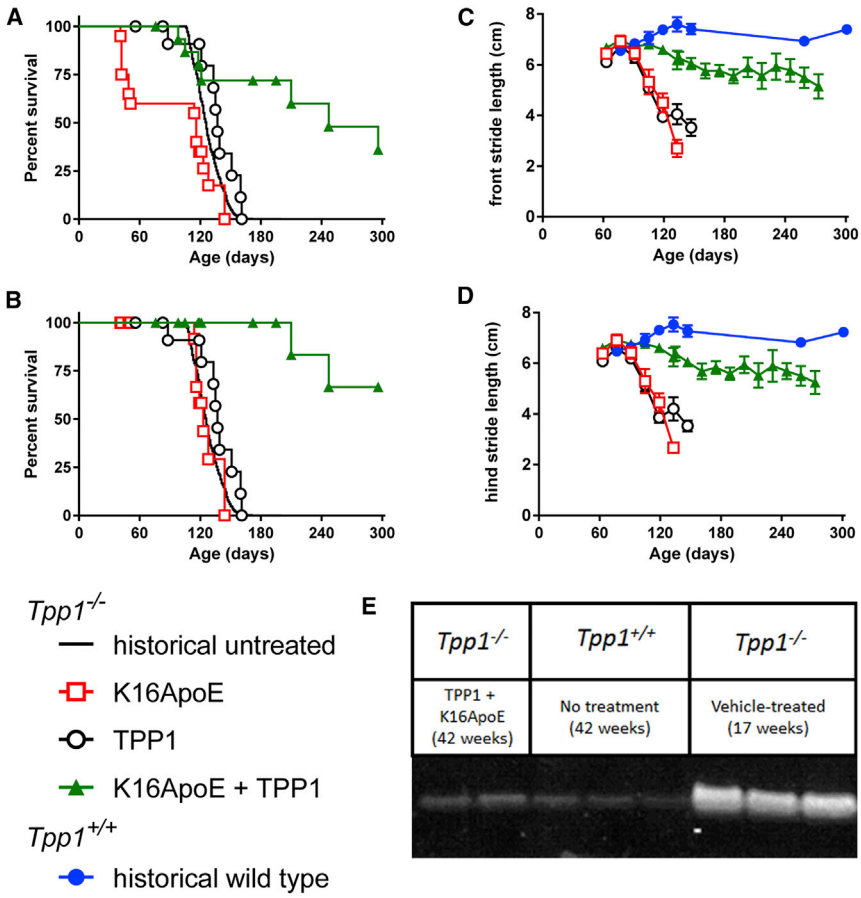

Figure 1. Chronic Therapy of Asymptomatic Animals Using Peptide-Mediated Delivery across the BBB

(A and B) *Tpp1*−/− mice were treated by tail vein injection with rhTPP1 alone (17 nmol or 1 mg; n = 20 animals), peptide K16ApoE alone (40 nmol or 180 μg; n = 13 animals), or a mixture of rhTPP1 and K16ApoE (n = 16 animals). Note that K16ApoE is frequently associated with infusion-related death. Given that this is independent of LINCL status, data are presented as the total (A) or with infusion-related deaths censored to indicate death due to disease (B). When compared to historical untreated animals, treatment significantly (log-rank test $p < 0.0001$) extended survival of the LINCL mouse, with or without censoring for infusion-related deaths. Gait analyses show mean stride length and bars represent SEM. (C) Front stride gait analysis. Difference in slope from wild-type animals: K16ApoE, $p < 0.0001$; rhTPP1, $p < 0.0001$; and rhTPP1 plus K16ApoE, $p = 0.0083$. (D) Hind stride gait analysis. Difference in slope from wild-type animals: K16ApoE, $p < 0.0001$; rhTPP1, $p < 0.0001$; and rhTPP1 plus K16ApoE, $p = 0.0048$. (E) Immunoblotting for SCMAS storage material.

was particularly efficient to the midbrain and hippocampus and less efficient to the anterior cerebral cortex (Figure 4). Fluorescent rhTPP1 was delivered efficiently to the cerebellum (Figure 2), reaching Purkinje cells both in the deep zone of the gyri and in surface proximal regions but again, delivery appeared more efficient to deeper regions. Fluorescence was punctate, cytoplasmic, and perinuclear, which again is consistent with delivery to the lysosome and/or other intracellular vesicles (see Figure 4, anterior cerebral cortex and brainstem). Neuronal staining was so extensive throughout the brain that identifying individual capillaries (as observed when fluorescent rhTPP1 is administered in the absence of K16ApoE, Figure 3) was difficult, although fluorescent rhTPP1 was detected in small blood vessels in some regions of relatively low staining (e.g., anterior cerebral cortex, Figure 4).

It is worth noting that in a recent study from our laboratory,[19] fluorescent rhTPP1 was delivered to the brain via the cerebrospinal fluid (CSF) using an intrathecal injection. Here, overall distribution of

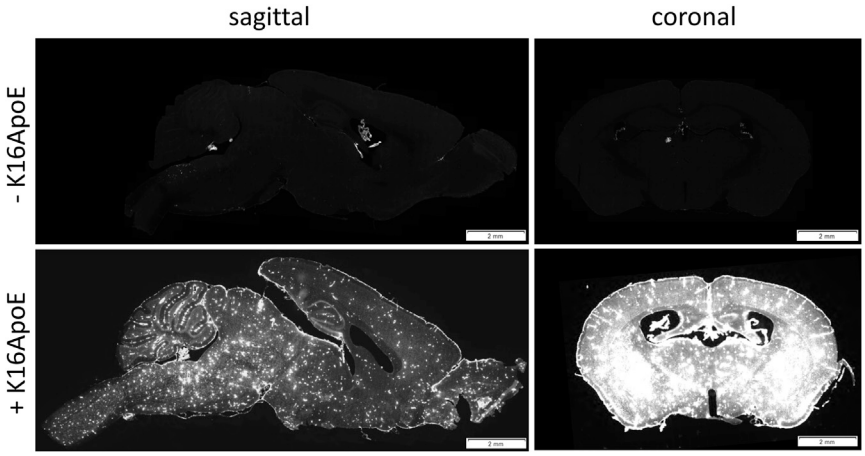

Figure 2. Distribution of Fluorescent rhTPP1 throughout the Brain after i.v. Delivery

C57BL/6 mice analyzed 18 hr after administration of 1 mg Alexa Fluor 647-labeled rhTPP1 with or without 40 nmol K16ApoE. Sections are shown using equivalent exposure settings. Scale bars represent 2 mm.

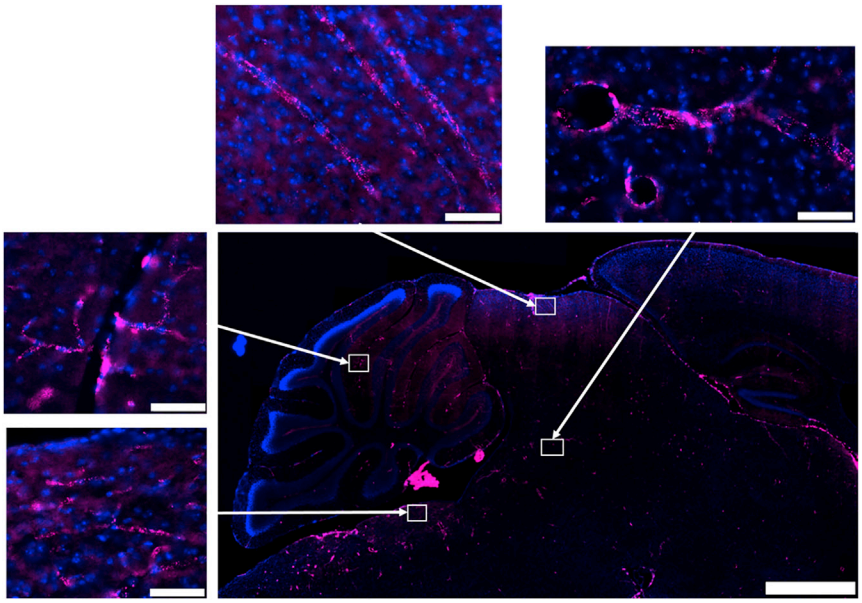

Figure 3. Distribution of Alexa Fluor 647-Labeled rhTPP1 in the Brain when Administered in the Absence of K16ApoE

Scale bars represent 1 mm for low-magnification panels and 50 μm for the higher-magnification panels that were imaged from the indicated brain regions (i.e., clockwise from the lower left: pons, cerebellum, dorsal midbrain, and central midbrain).

rhTPP1 was quite uneven, with the most efficient delivery to ventral surfaces of the brain and very poor or undetectable delivery to dorsal and deep brain regions, such as the hippocampus. Distribution of rhTPP1 using the peptide-mediated i.v. route was markedly more uniform with widespread delivery throughout the brain.

Insights into Peptide-Mediated Brain Delivery

To gain insights into the mechanism of action of K16ApoE, we followed the fate of a fixable tracer, sulfo-NHS-biotin, by microscopy after probing with fluorescent streptavidin. Mice were anesthetized with a sublethal dose of Euthasol, administered K16ApoE at t = 0, administered tracer at t = 1 min, euthanized by exsanguination at t = 2 min, and processed for microscopy and biotin was visualized by staining with Alexa Fluor 554-labeled streptavidin. Times were chosen so that the experiment could be terminated before animals died when administered high doses of peptide. Little fluorescence is detected in the absence of K16ApoE. Fluorescence increases with peptide dose, showing bright staining characteristic of the vasculature

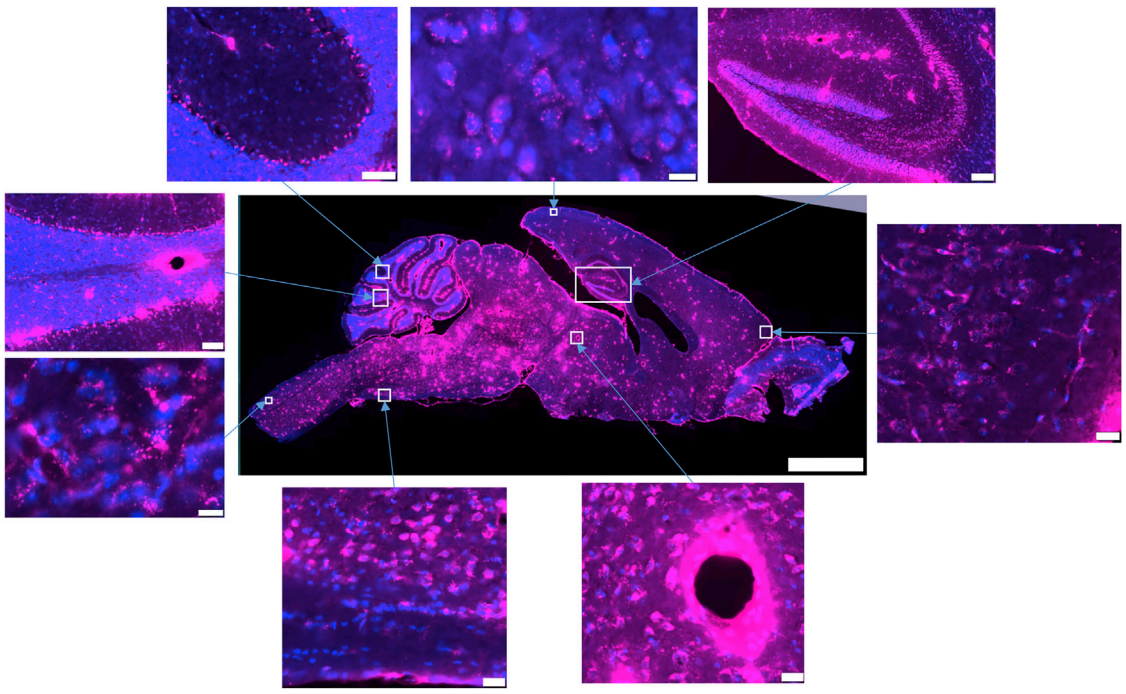

Figure 4. Distribution of Alexa Fluor 647-Labeled rhTPP1 in the Brain when Administered in the Presence of K16ApoE

Scale bars represent 2 mm for the low-magnification panels and the following for the higher-magnification panels (i.e., clockwise from the top right): hippocampus, 100 μm; anterior cerebral cortex, 20 μm; midbrain, 20 μm; ventral medulla, 20 μm; brainstem, 10 μm; cerebellum (lobe VIII), 50 μm; cerebellum (lobes VI/VII), 50 μm; and posterior cerebral cortex, 10 μm.

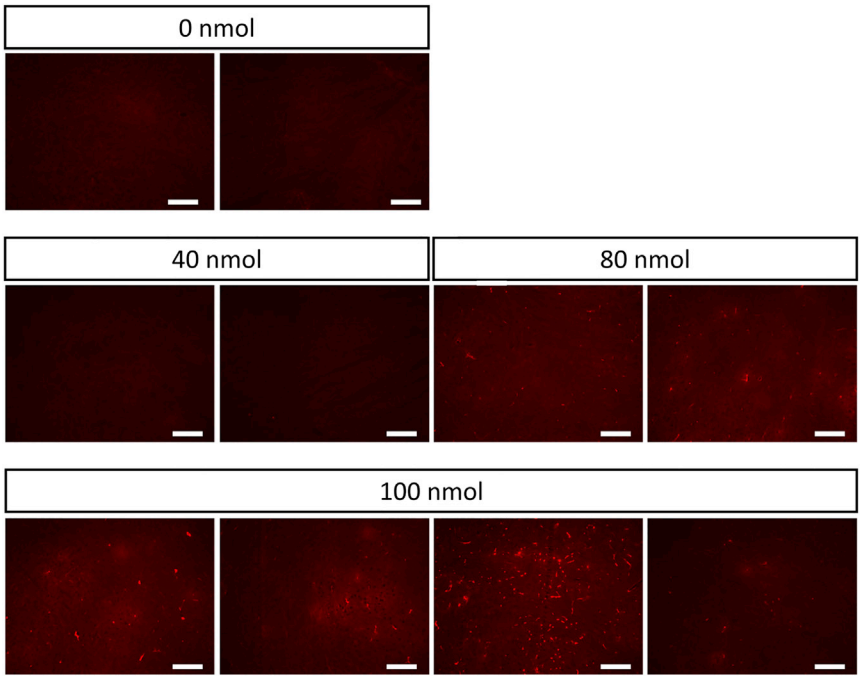

Figure 5. Effect of Increasing Dose of K16ApoE on Distribution of NHS-Biotin, an i.v. Fluid Phase Tracer
Scale bars represent 200 μm, and sections are imaged within the frontal cortex.

as well as faint staining throughout the parenchyma (Figure 5). This is consistent with K16ApoE promoting endocytosis of the tracer into endothelial cells followed by transcytotic release from the abluminal surface into cells proximal to the vasculature.

Time-course experiments were conducted to follow the distribution of a fluorescent rhTPP1 derivative and fluorescein isothiocyanate (FITC)-K16ApoE, a peptide with similar brain-targeting properties as K16ApoE (see below). Based on morphological criteria, we classified fluorescence as being associated with either blood vessels or parenchyma (Figure 6). K16ApoE and rhTPP1 derivatives both appear in blood vessels throughout the brain as well as in the parenchyma. At later times, the signal from the peptide disappears but the rhTPP1 persists. This is consistent with the peptide being degraded and the rhTPP1 persisting within the cell.

We conducted experiments to determine the pharmacokinetics of rhTPP1 uptake. Radiolabeled rhTPP1 and the vascular space marker albumin were co-administered to wild-type mice via jugular vein injection in the presence or absence of K16ApoE and/or unlabeled rhTPP1. The ^{131}I-labeled albumin was cleared slowly from the bloodstream in all cases (Figure 7A, open symbols). For ^{125}I-labeled rhTPP1, bloodstream clearance was not affected by K16ApoE, while the unlabeled rhTPP1 inhibited clearance, probably due to saturation of receptor-mediated uptake systems (e.g., mannose 6-phosphate [M6P] and mannose receptors). This is supported by analysis of the liver and spleen, where unlabeled rhTPP1, but not K16ApoE, inhibited uptake of ^{125}I-rhTPP1, with ^{131}I-albumin uptake being low in all cases.

In the brain, K16ApoE had a striking effect in enhancing uptake of ^{125}I-rhTPP1 (Figure 7B). It is worth noting that for the injections of tracer alone, some ^{125}I-rhTPP1 accumulated in the brain. The addition of unlabeled rhTPP1 in the absence of K16ApoE reduced brain uptake to levels seen with albumin (Figure 7B). This suggests that small amounts of rhTPP1 can be delivered to the brain by a saturable transport system. The enhanced uptake induced by K16ApoE was also reduced by the addition of unlabeled rhTPP1. This suggests that K16ApoE could be enhancing the endogenous mechanism of uptake for rhTPP1.

The presence of K16ApoE also appeared to result in an increase in the amount of ^{131}I-labeled albumin tracer entering the parenchyma in the absence or presence of rhTPP1 ($p = 0.052$ and 0.064, respectively, after Bonferroni correction for multiple comparisons) (Figure 7C). To investigate this further, we conducted a mass spectrometry-based measurement of albumin in the brain of animals treated with rhTPP1 and increasing amounts of K16ApoE. Levels of a control protein (beta-actin) in the brain were unaffected by treatment with K16ApoE (Figure 8A). However, there was a K16ApoE dose-dependent increase in albumin within the brain (Figure 8B) that paralleled uptake of rhTPP1 (Figure 8C). Comparison of albumin levels and rhTPP1 activity in individual animals indicated that they were strongly correlated ($r^2 = 0.604$). K16ApoE had no significant effect on uptake of rhTPP1 or albumin to the liver or kidney (Figures 7C–7G).

A reasonable candidate for the K16ApoE-mediated uptake of rhTPP1 into the parenchyma of the brain is the cation-dependent M6P receptor (M6PR), which can transport proteins across the BBB.[20,21] We investigated this possibility by co-injecting rhTPP1 and K16ApoE with free M6P to block interaction with the M6PR (Figure 9). K16ApoE effectively mediated uptake of rhTPP1 into the parenchyma of the brain (Figure 9A), but the presence of free M6P had no significant effect. As before, K16ApoE did not affect uptake of rhTPP1 by the liver and kidney, and this was unaffected by coadministration of M6P (Figures 9B and 9C). These results suggest that K16ApoE is not operating in conjunction with the M6PR to promote rhTPP1 passage across the BBB. However, it is possible that the concentration of free M6P (0.2 mM) was insufficient to prevent M6PR-mediated uptake of rhTPP1 to the brain, although this concentration was sufficient to inhibit uptake of β-glucuronidase in similar studies.[22]

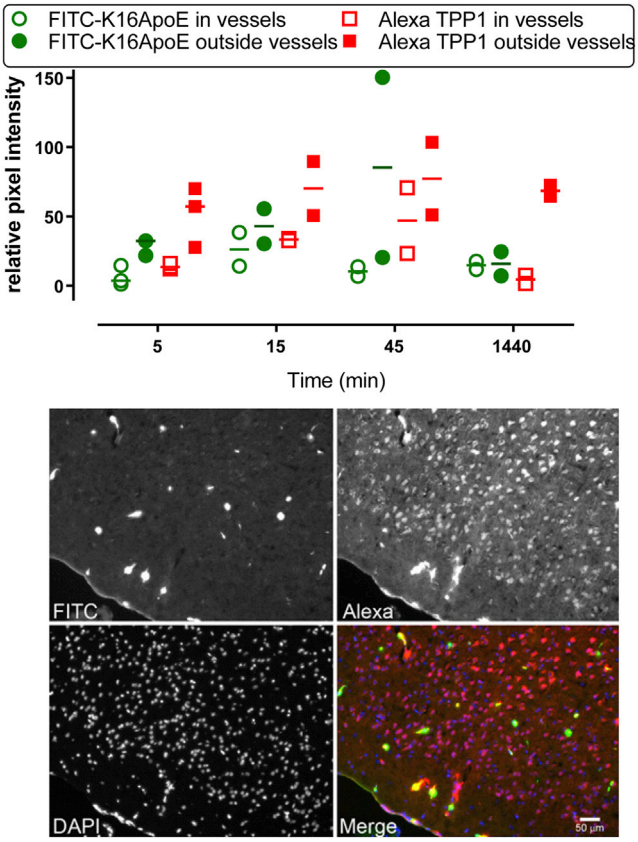

Figure 6. Distribution of Peptide and Protein in the Brain

Animals were co-administered Alexa Fluor 594-rhTPP1 (1 mg) and FITC-K16ApoE (40 nmol) by tail vein injection. (Top) Quantification of peptide and protein within and outside blood vessels. (Bottom) Micrographs of the cerebral cortex of an animal euthanized 45 min after administration.

In analyses of the whole brain by enzyme assay, it is not possible to distinguish between rhTPP1 that has reached the parenchyma versus enzyme associated with the vascular compartment (e.g., sequestered within or weakly bound to the luminal surface of brain endothelial cells [BECs]). Using a capillary depletion method performed with or without vascular washout,[23,24] we were able to distinguish the distribution of ^{125}I-labeled rhTPP1 among three compartments (Table 1): (1) that which crossed the BBB completely to enter the parenchyma of the brain, (2) that which was taken up by the BEC but not completely transcytosed (sequestered), and (3) that which reversibly adhered to the luminal surface of the BEC but was not internalized by it (luminal adherence). In the absence of K16ApoE, relatively little rhTPP1 entered the parenchyma of the brain but was mostly adhered to the luminal surface or sequestered by the BEC. With K16ApoE coadministration, most of the ^{125}I-labeled rhTPP1 entered the parenchymal space of the brain. These data are consistent with Figure 9 and demonstrate that K16ApoE mediates the passage of rhTPP1 across the BBB into the parenchyma of the brain.

Structure-Function Relationships

We evaluated a series of K16ApoE variants (Table 2) to help understand the mechanisms of action and toxicity, with the hope of identifying less toxic but still effective mediators of BBB transport. In initial studies, we conducted dose-response experiments in LINCL mice, co-administering rhTPP1 with increasing amounts of peptide until reaching a dose where animals died. Here, the highest amount of peptide represents the maximum tolerated dose (MTD) (Figure 9A). In subsequent experiments, we first determined the MTD in wild-type animals, and we then analyzed efficacy at the MTD in LINCL mice (Figure 9B).

K16ApoE was originally envisaged[8] to non-covalently associate with target proteins via the polylysine sequence and mediate passage by binding to members of the low-density lipoprotein (LDL) receptor family on BECs via a 20-amino-acid segment corresponding to residues 133–152 of ApoE. To investigate the specificity of the proposed receptor interaction, we varied amino acids in ApoE residues 130–149, as others have used peptide variants in this region to characterize binding to the LRP1 extracytoplasmic domain in vitro.[25] A peptide [K16ApoE(130–149)] in which the 133–152 ApoE sequence of K16ApoE was substituted with the wild-type 130–149 ApoE sequence was as effective as K16ApoE in promoting rhTPP1 uptake across the BBB (Figure 10A). Peptides containing changes predicted to diminish receptor binding of K16ApoE(130–149), a variant containing a lysine to glutamic acid change (K143E) and a scrambled variant, were also effective in promoting brain delivery of rhTPP1 in vivo, and both also exhibited toxicity (Figure 10A).

These results question the specific interaction of K16ApoE with LDL receptor family members but cannot discount interaction with other molecules expressed on the luminal side of the BEC. For example, the ApoE segment binds heparin[25] and other anionic GAGs via two heparin-binding motifs (XBBXB or XBBBXXBX, where B is a basic and X is any amino acid). K16ApoE(130–149) scram retains one heparin-binding motif; thus, we could not preclude the possibility of GAG binding. We addressed this possibility in two ways. First, we tested a randomized ApoE peptide in which the basic amino acids are spaced so that all consensus heparin-binding sites are eliminated (K16ApoE_rand). This peptide was also toxic and did promote rhTPP1 transport into the brain, although possibly with lower efficacy than other peptides. Second, based on a recent study[26] on the role of tryptophan residues in binding of GAGs, we replaced ApoE with a cell-penetrating peptide sequence that binds GAGs efficiently (R10W6). This peptide was also both functional and toxic.

We also tested N-terminally modified K16ApoE derivatives containing FITC, tetramethylrhodamine (TAMRA), and a 12-unit polyethylene glycol (PEG12) polymer. All had brain-targeting activity and were toxic. Finally, we explored the effect of replacing the polylysine tract with polyarginine or polyhistidine. R16ApoE was similar to K16ApoE in terms of efficacy and toxicity. In contrast, H16ApoE was non-toxic but it had no brain-targeting activity at the highest

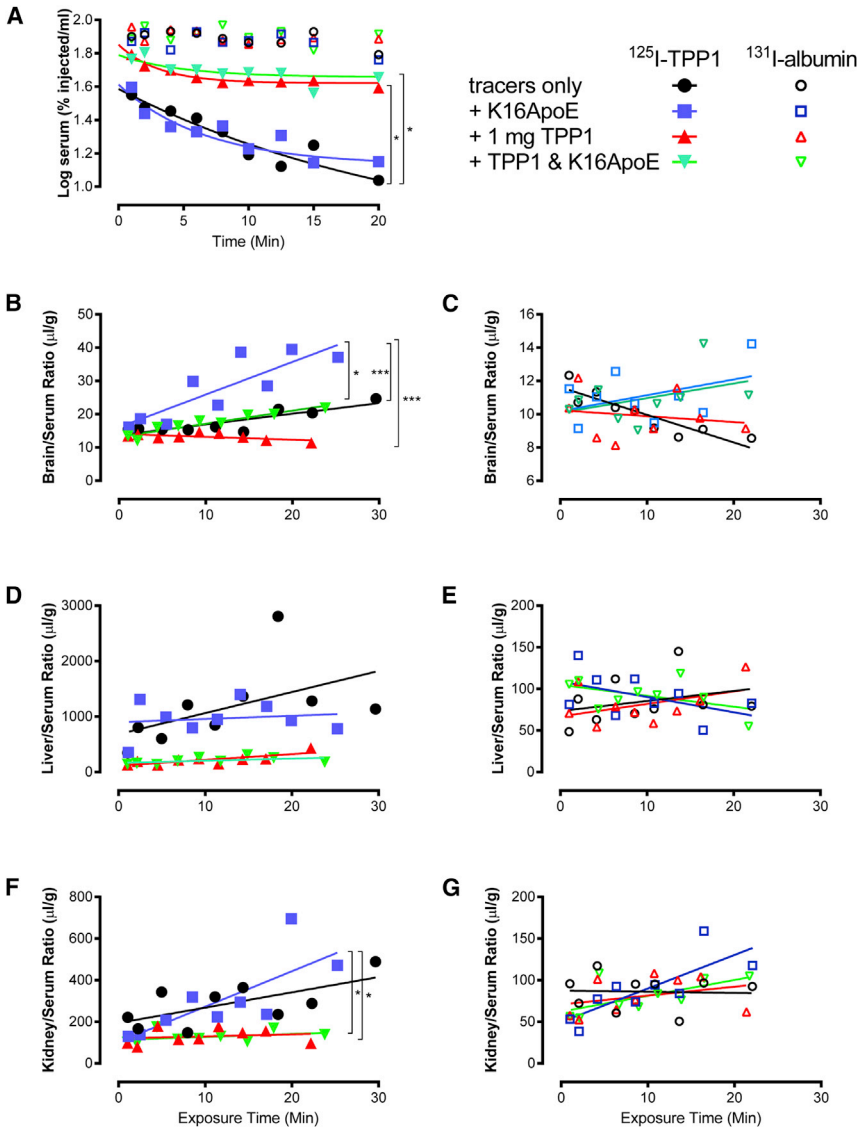

Figure 7. Effect of K16ApoE and Unlabeled rhTPP1 on ^{125}I-rhTPP1 and ^{131}I-Albumin Pharmacokinetics

Ten-week-old CD-1 male mice were administered 1×10^6 cpm of each tracer in the presence or absence of 40 nmol K16ApoE and/or 1 mg unlabeled rhTPP1. (A) Clearance of labeled tracer albumin and rhTPP1 from serum. Clearance of albumin is unaffected by the presence or absence of unlabeled rhTPP1 and/or K16ApoE. The presence of K16 had no significant effect on clearance of tracer with or without unlabeled rhTPP1. However, the addition of unlabeled rhTPP1 significantly slowed clearance of tracer with or without K16ApoE. (B–G) Uptake of labeled tracer rhTPP1 or albumin is shown as the ratio to serum levels for the brain (B and C), liver (D and E), and kidney (F and G). p values were determined by linear regression in a combined model, and significance is indicated by *$p < 0.05$; ***$p < 0.005$ after Bonferroni correction for multiple comparisons. Note that K16ApoE significantly ($p = 0.04$, one-tailed t test with no assumptions about variance) promotes uptake of rhTPP1 to wild-type CD-1 mice, with levels in treated animals (n = 3) being 1.5-fold higher than in untreated animals (n = 2).

doses tested. Taken together, the analysis of variant peptides suggested that toxicity and the ability to promote passage across the BBB were intrinsically linked.

Underlying Basis for Toxicity

In a cultured cell-based assay, Chinese hamster ovary (CHO) cells were incubated with K16ApoE and its derivatives and cell death was measured using the fluorescent exclusion dye propidium iodide, which fluoresces when it binds DNA within the nucleus of dead and dying cells that lack an intact plasma membrane. In a kinetic assay (Figure 11A), K16ApoE promoted cell death in a dose- and time-dependent manner. Using an endpoint assay (Figure 11B), we found that K16ApoE, R16ApoE, and K16R10W6 all promoted cell death in a similar manner. In contrast, and consistent with in vivo data, H16ApoE failed to induce cell death.

Animals administered toxic doses of K16ApoE exhibited agonal breathing, and the time to death decreased with the increasing peptide dose. We conducted a number of observational and pilot experiments aimed at uncovering the basis for toxicity of K16ApoE and related peptides, with the hope that this information might provide a route toward an improved therapeutic index. While these endeavors were not successful, we believe that it is worth briefly describing these studies to help rule out potential mechanisms for toxicity as well as approaches to circumvent toxicity. Experimental details and results are included in Table S1.

First, comprehensive necropsy failed to reveal any apparent cause of death. While microcapillary occlusion in the lungs due to erythrocyte agglutination has been proposed to be a possible cause of death with other cationic peptides,[14,15] there were no remarkable changes observed in the lungs of animals that died as a result of acute K16ApoE toxicity. No microthrombi were observed in alveolar capillaries and no edema was present in the alveoli. Second, no pathological changes attributable to K16ApoE could be detected even after prolonged treatment of LINCL mice (36 weekly doses of 1 mg rhTPP1 and 40 nmol K16ApoE). Third, no abnormal electrical activity preceding death was observed when recording electroencephalograms (EEGs) using surface and deep hippocampal electrodes. Fourth, we considered the possibility that death in response to K16ApoE could be due to an acute anaphylactoid response, given that this is not uncommon with cationic drugs. In mice, the inflammatory response to cationic compounds, including basic peptides, is mediated by the receptor Mrgprb2.[27] Indeed,

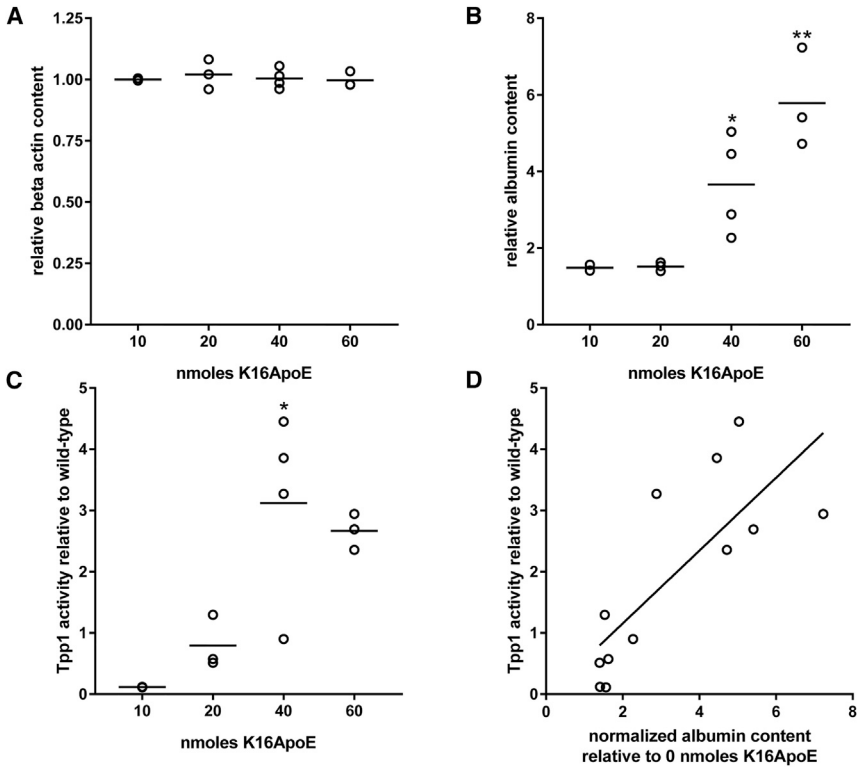

Figure 8. K16ApoE-Mediated Uptake of Albumin to the Brain

LINCL mice were treated with 1 mg rhTPP1 and the indicated amounts of K16ApoE. (A and B) K16ApoE-mediated uptake to the brain was measured for beta-actin (A) and albumin (B) by mass spectrometry-based analysis of brain extracts. Raw spectral count data were normalized to total spectral counts per sample and then expressed relative to average levels measured in untreated LINCL mice (n = 2). (C) TPP1 activities in the same animals were measured by enzyme assay and are normalized to wild-type animals. (D) TPP1 activity and albumin content are correlated ($r^2 = 0.604$). p values were measured for comparisons with untreated LINCL mice (albumin and beta-actin) or animals treated with the lowest dose of K16ApoE (Tpp1 activity) using one-way ANOVA with the Dunnett multiple-comparisons test. *$p < 0.05$; **$p < 0.001$.

K16ApoE induced degranulation of mouse mast cells in an Mrgprb2-dependent manner (B. McNeil, personal communication). However, death due to K16ApoE was at least as rapid in knockout mice lacking Mrgprb2 compared to controls, suggesting that a response other than anaphylaxis was responsible for toxicity. Fifth, while unlikely, we addressed the possibility that death was due to unobserved microinfarctions by co-injecting the anionic indirect thrombin inhibitor fondaparinux with K16ApoE. This prevented death, but it also prevented K16ApoE from promoting brain delivery of co-administered rhTPP1. We speculate that this anionic agent neutralizes the highly positive charge of K16ApoE and, in doing so, ameliorates both desired and adverse effects. Similar results have been reported with coadministration of K16ApoE with other negatively charged drugs.[28] Subcutaneous administration of the indirect thrombin inhibitor enoxaparin did not prevent K16ApoE toxicity. Finally, we investigated the possibility that increased amounts of protein delivered with K16ApoE could abrogate toxicity by competing for binding to the BBB. However, coadministration with large amounts of TPP1 (17 mg) or albumin (85 mg) failed to attenuate toxicity, indicating that this is not the case.

DISCUSSION

While K16ApoE mediated the therapeutically effective delivery of rhTPP1 to lysosomes throughout the mouse brain, our efforts to identify variants that retained efficacy but were less toxic were not successful. This suggests that the inherent toxicity of K16ApoE is linked with, and possibly underlies, its ability to mediate protein passage across the BBB. Therefore, we instead made significant efforts toward understanding the mechanism of K16ApoE action with the hope that this knowledge might provide a route toward a safer drug. Results were again consistent with mechanism-based toxicity. For example, co-treatment with negatively charged compounds allowed mice to survive fatal doses of K16ApoE but the ability to transport rhTPP1 across the bloodstream was lost.

K16ApoE was designed[8] to non-covalently associate with target proteins via the polylysine sequence and mediate passage by binding to members of the LDL receptor family on BECs via a 20-amino-acid segment of apolipoprotein E. Earlier, we found that delivery to the brain was similar when K16ApoE was premixed and co-administered with rhTPP1 or injected separately, either immediately prior to or after rhTPP1 administration.[3] This suggested that in vivo, K16ApoE does not exclusively function by direct association with rhTPP1. Further evidence that K16ApoE does not function in the manner originally envisaged comes from the observation here that randomization of the ApoE LDL receptor binding sequence or specific amino acid changes to eliminate receptor binding do not prevent its ability to promote rhTPP1 delivery across the BBB. In addition, modification of K16ApoE to eliminate canonical GAG binding motifs still resulted in some delivery of rhTPP1 across the BBB.

While the mechanism of action of K16ApoE remains unknown, there is no obvious specificity to the proteins that are transported into the brain. In addition to rhTPP1, previous studies have demonstrated that K16ApoE can also mediate the uptake of bacterial β-galactosidase, immunoglobulin G (IgG), and immunoglobulin M (IgM)[8]; here, we show that K16ApoE facilitates delivery of albumin to the brain (Figures 7 and 8). K16ApoE may function, at least in part, by stimulating adsorptive-mediated transcytosis,[29–31] which relies on

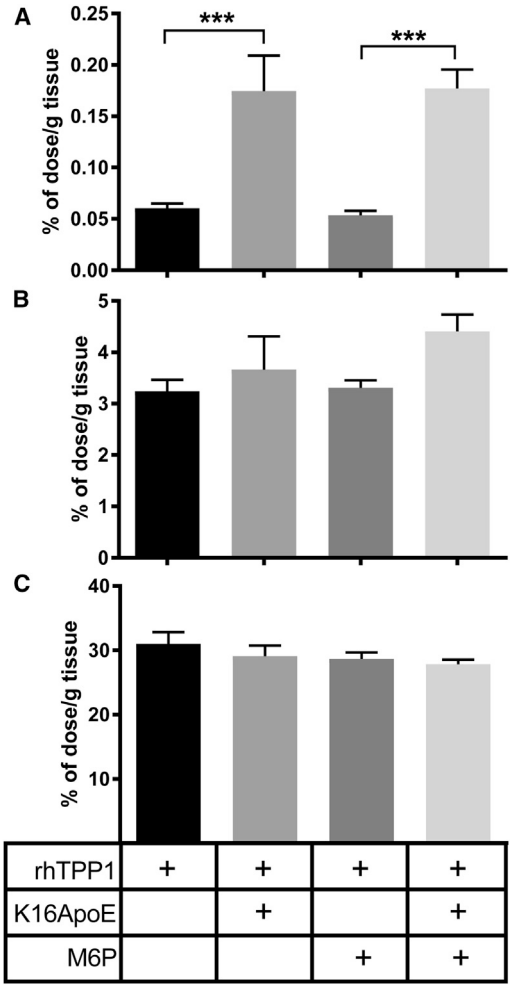

Figure 9. Effect of M6P on Peptide-Mediated Uptake of rhTPP1

(A–C) Mice were administered rhTPP1, with or with K16ApoE, in a total volume of 200 μL PBS containing 1 mM M6P (n = 4–8 animals per group) and were euthanized 10 min after injection. Data show the percentage of injected dose per gram of each tissue, corrected for vascular contribution using ^{99m}Tc-labeled albumin as a standard that is still largely retained in plasma after 10 min. Error bars represent the SEM for the brain (A), kidney (B), and liver (C). Significance was determined using pairwise t tests corrected for multiple comparisons using the Holm method. ***$p < 0.005$.

positively charged regions of a molecule interacting with negative charges on the plasma membrane, resulting in invagination, internalization of vesicles, and vesicular transport to the abluminal membrane.[32] This transport would first result in preferential endocytosis of molecules bound to the luminal surface but results in vesicle-based transport when stimulated sufficiently, effectively causing flux of solutes across the BBB at rates that may result in toxicity. Alternatively, an increased level of membrane trafficking could result in a loss of polarity of endothelial cells, resulting in paracellular transport.

In conclusion, evidence to date indicates that K16ApoE toxicity and efficacy are linked, as different avenues to obviate toxicity either were unsuccessful or resulted in the loss of rhTPP1 transport into the brain. This precludes clinical development of the approach at this time. However, it is possible that covalent or other attachment of K16ApoE to target molecules like rhTPP1 may facilitate uptake while diminishing the toxicity associated with the large molar excess of free peptide to which animals are exposed using our current methods. Regardless, the approach still has considerable value for proof-of-principle studies of bloodstream-mediated enzyme replacement therapy to the brain for LINCL, other LSDs, and possibly more widespread diseases. In addition, peptide-mediated delivery also provides a useful route for the initial evaluation of potentially improved protein therapeutics for the brain prior to studies using more demanding but clinically relevant delivery methods (e.g., intrathecal or intracerebroventricular injection). However, development of methodology to safely achieve delivery across the BBB remains a key goal, given relatively non-invasive administration and the broad distribution that can be achieved throughout the brain that may not necessarily be achievable by CSF-mediated delivery strategies.

Table 1. Effect of K16ApoE on Distribution of rhTPP1 in the Mouse Brain

Distribution	rhTPP1 Tissue/Serum Ratio (μL/g)	
	Without K16ApoE	With K16ApoE
Parenchyma penetration	1.25 ± 0.17	7.68 ± 1.24
Capillary sequestration	0.94 ± 0.48	2.15 ± 0.28
Luminal adherence	1.97 ± 0.44	1.67 ± 1.31

Capillary depletion studies done with and without vascular washout determined the ^{125}I-labeled rhTPP1 with or without K16ApoE that entered brain parenchyma, was sequestered by the capillary, or was adherent to the luminal surface of the capillary. Data are corrected for vascular space using ^{99m}Tc albumin as a protein that remains largely in the luminal space in the presence and absence of K16ApoE (see Figure 7). Two animals were used for each of the four conditions, Data are shown as the mean ± compounded SEM. $p = 0.036$ for parenchymal penetration using a two-tailed t test without multiple comparison correction.

MATERIALS AND METHODS

Materials

rhTPP1 proenzyme in artificial CSF at a concentration of 29 mg/mL was generously provided by BioMarin and was buffer exchanged to PBS before administration. Fluorescent Alexa Fluor 647-labeled rhTPP1 was generated by reaction with Alexa Fluor 647 N-hydroxysuccinimide (NHS) ester (Thermo Fisher Scientific) and purified by buffer exchange using PD10 columns. Labeling efficiency was 0.7 mol dye/mol rhTPP1 based on absorbance using molar extinction coefficients of ε280 = 82,195 for rhTPP1 and ε280 = 7,170 and ε467 = 239,000 for Alexa Fluor 647. Peptides were synthesized by LifeTein.

Animals

Animal maintenance and use followed protocols approved by the Robert Wood Johnson Medical School Institutional Animal Care and Use Committee ("Preclinical Evaluation of Therapy in an Animal Model for LINCL," protocol I09-0274-4). *Tpp1*$^{-/-}$ mice were genotyped as described previously[4] and were in a C57/BL6 background.

Table 2. K16ApoE and Peptide Variants

Peptide	Sequence
K16ApoE	K_{16}LRVRLASHLRKLRKRLLRDA
K16ApoE(130–149)	K_{16}TEELRVRLASHLRKLRKRLL
K16ApoE(130–149)K143E	K_{16}TEELRVRLASHLRQLRKRLL
K16ApoE(130–149)scram	K_{16}LREKKLRVSALRTHRLELRL
K16ApoE_rand	K_{16}RAKDRARLRLRVRLKLHLSL
K16R10W6	K_{16}RRWWRRWRRWRRWWRR
R16ApoE	R_{16}LRVRLASHLRKLRKRLLRDA
H16ApoE	H_{16}LRVRLASHLRKLRKRLLRDA
PEG12-K16ApoE	PEG12-K_{16}LRVRLASHLRKLRKRLLRDA
TAMRA K16ApoE	TAMRA-K_{16}LRVRLASHLRKLRKRLLRDA
FITC-K16ApoE	FITC-K_{16}LRVRLASHLRKLRKRLLRDA

Numbering in parentheses is based on mature human ApoE.

Mice were anesthetized with isoflurane using an anesthesia inhalation system (VetEquip) and were administered rhTPP1 and/or K16ApoE in 200 µL PBS by tail vein or retro-orbital injection. Animals were pretreated by intraperitoneal administration of 5 mg/kg cyproheptadine to prevent infusion-related anaphylaxis from the second or third dose onward. Mice were housed singly from age 6 weeks (asymptomatic animals) and were gently handled to avoid fatal startle seizures.[4] Locomotor function was measured by biweekly gait analysis.[33] Animals anesthetized with Euthasol (pentobarbital sodium and phenytoin sodium, Delmarva Laboratories) were euthanized by exsanguination/transcardial perfusion with PBS and dissected. Half of the brain was rapidly frozen for enzyme activity and other biochemical analyses and the other half was drop-fixed in 4% paraformaldehyde (PFA) for histopathology as described.[3] To determine whether administered fluorescent rhTPP1 crossed the capillary wall of the brain vasculature to enter the brain parenchyma, capillary depletion[24] was conducted as modified for the mouse.[23]

For imaging experiments using fluorescent rhTPP1 or NHS-sulfo-biotin, the PBS perfusion was followed by perfusion with 4% PFA. Sections were prepared for whole-slide imaging as described.[19] Biotin staining was conducted as described.[34]

Experimental Design for Survival and Gait Studies

Survival and gait data were obtained using three concurrent cohorts of LINCL mice that were treated with rhTPP1 and K16ApoE, or either rhTPP1 or K16ApoE alone. Survival data were compared to historical results from 1,560 untreated C57BL/6 LINCL mice, while stride-length data were compared to an earlier analysis of a cohort of wild-type animals. Our experimental plan was to allow most animals to die naturally but to euthanize two at an early 119-day time point (17 weeks) and all survivors at a predetermined study endpoint of 294 days (42 weeks), for biochemical and histopathological analyses.

Gait was analyzed using a random-effects model fitted to the stride data, with "stride" as the response variable and "days" as the predictor, with separate predictions for each of the four animal types. In the hierarchical model, observations were nested within animals. The "lme" function in the "lmerTest" R package (R Project for Statistical Computing) was used to fit the random-effects model.

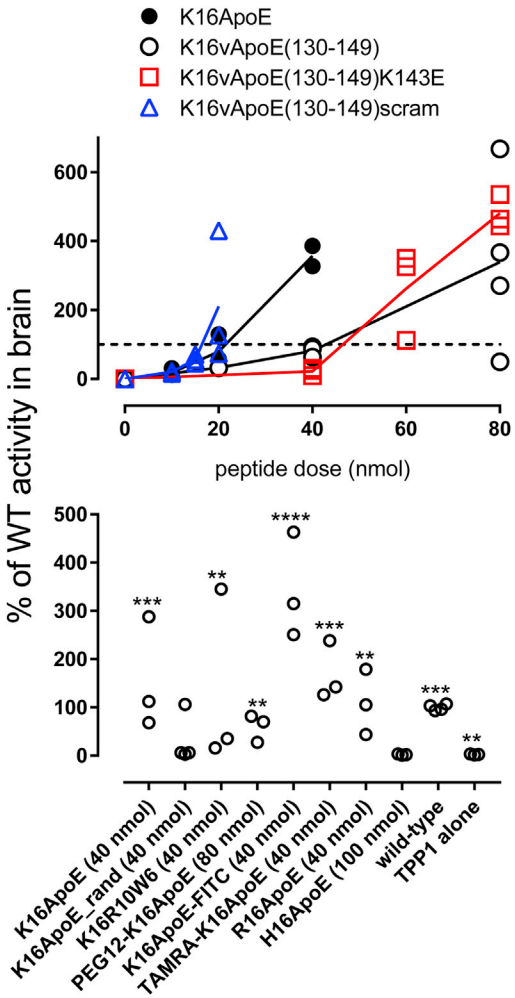

Figure 10. Efficacy of K16ApoE Variant Peptides

LINCL mice were treated with i.v. injection of 17 nmol (1 mg) rhTPP1 with the indicated peptide doses in a volume of 200 µL. Mice were euthanized 24 hr later and TPP1 activity was measured in the brain. Two or three animals were used per peptide dose. (A) Dose response for selected peptides. The highest dose shown is the MTD, as 2-fold higher levels resulted in toxicity. (B) Variants tested at MTD (indicated) except H16ApoE, which was not toxic and was tested at 100 nmol. The dashed line represents 100% wild-type activity. Note that peptide amounts were based on weight of synthetic peptides and should be considered approximate. Three animals were used per peptide. Significant differences in rhTPP1 uptake with peptide variants compared to treatment with rhTPP1 alone were determined using one-way ANOVA with the Dunnett multiple-comparisons test. **$p < 0.01$; ***$p < 0.005$; ****$p < 0.001$. WT, wild type.

Microscopy

For imaging experiments using fluorescent rhTPP1, animals were perfused and sections were prepared for whole-slide imaging as

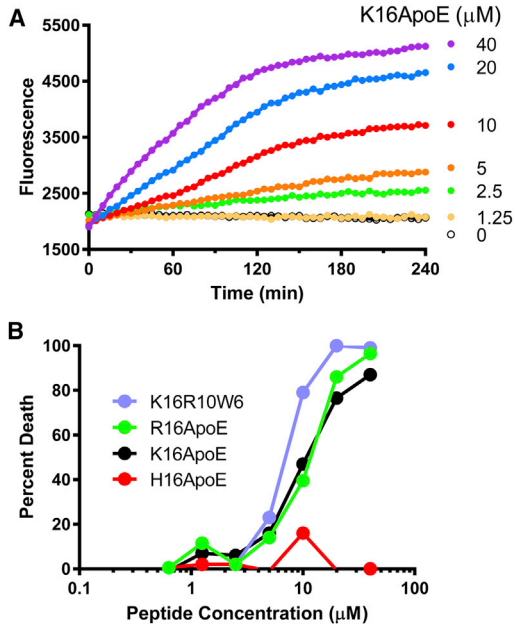

Figure 11. Cytotoxicity of K16ApoE

(A) Kinetic assay. CHO-K1 cells were cultured in DMEM complete medium (with 10% fetal bovine serum, 100 U/mL penicillin, 100 μg/mL streptomycin, and 2 mM L-glutamine) containing 20 μM propidium iodide and the indicated concentrations of K16ApoE. Fluorescence was monitored at 1-min intervals. (B) Endpoint assay. CHO-K1 cells in complete medium with propidium iodide were cultured with the indicated concentration of peptide for 2 hr. Fluorescence was determined before the addition of peptide (Fo), after incubation with peptide (Fp), and after cells were permeabilized with digitonin (Fd). Cell death is calculated as (Fp − Fo)/(Fp − Fd).

described previously in detail.[19] Whole-slide images were acquired using an Olympus VS120 whole-slide scanner equipped with an Olympus XM10 cooled monochrome 14-bit camera. NHS-sulfo-biotin staining was conducted as described.[34]

SCMAS Immunoblotting

Mouse brain samples were homogenized in 1:50 volumes (w/v) of 0.15 M NaCl/0.1% Triton X-100 using a Polytron tissue homogenizer (Kinematica). One hundred microliters of each homogenate (~1.5 mg protein/mL) was centrifuged at 14,000 × *g* for 30 min to fractionate the insoluble storage material containing SCMAS. Pellets were resuspended in 100 μL homogenization buffer and re-centrifuged. The pellet was dissolved in reducing lithium dodecyl sulfate PAGE buffer and 4- and 8-μg equivalents of the initial homogenates were analyzed by immunoblotting as described.[6]

Pharmacokinetic Studies

rhTPP1 was radioactively labeled with ^{125}I using the lactoperoxidase method and separated from unincorporated iodine over a column of G-10 Sephadex (GE Healthcare).[35] Albumin was radioactively labeled with ^{131}I using the chloramine T method[36] or with ^{99m}Tc[37]; in both cases, labeled rhTPP1 was separated from the unincorporated label over a column of G-10 Sephadex.[36] Mice were anesthetized with urethane given intraperitoneally and the right jugular vein and the left carotid artery exposed. Mice received an injection into the jugular vein of lactated Ringer's solution containing 10^6 cpm ^{125}I-rhTPP1 and 10^6 cpm ^{131}I-albumin with or without 40 nmol K16ApoE or 1 mg unlabeled rhTPP1. The carotid artery was severed between 1 and 20 min after the i.v. injection, arterial blood was collected, and the mouse was immediately decapitated. The arterial blood was centrifuged and 50 μL arterial serum was obtained for determination of the levels of radioactive ^{125}I and ^{131}I. Whole brains, a kidney, and a portion of liver were removed and weighed, and the levels of these isotopes were determined using a gamma counter. Tissue/serum ratios were determined and plotted against exposure time to determine the unidirectional uptake rate using multiple-time regression analysis.[38,39]

Statistical Analyses

Statistical analyses were conducted using Prism 5.03 (Graph-Pad Software) and R 3.3 software.[40]

EEG Analysis

Female B57/Bl6 mice were implanted with a hippocampal-depth electrode (six-pin surface mount connector; Pinnacle Technology) placed at 2.2 mm posterior to the bregma, 1.7 mm lateral to the midline at a depth of 2.0 mm under continuous isoflurane anesthesia (2% in 95% O_2 and 5% CO_2) delivered through a nose cone. Video-EEG recordings were performed 5 days after electrode implantation. Following 10-min baseline EEG recording using a 100× gain preamplifier system (8200-K1-iSE3; Pinnacle Technology), K16ApoE was injected and the EEG was monitored for electrographic seizures. Electrographic seizures were defined as repetitive spike and sharp-wave discharges with a frequency of > 1 Hz, amplitude of activity more than two times over baseline with a duration > 5 sec.[41]

TPP1 Assay

Mouse brain extracts were prepared in 0.15 M NaCl /0.1% Triton X-100 and TPP1 activity was measured and normalized to the protein concentration as described previously.[3]

Mass Spectrometry

To determine the relative albumin content, a 10-μg protein equivalent of each extract was fractionated by SDS-PAGE and digested in-gel with trypsin and peptides were extracted as described.[42] Data-dependent mass spectrometry was conducted on duplicate 0.5-μg protein equivalents of digested peptides using a Thermo Scientific LTQ Orbitrap Velos mass spectrometer, protein assignment was conducted using a local implementation of the GPM,[43] and relative albumin levels were calculated by spectral counting[44] after normalization to the total spectral counts assigned to each sample.

SUPPLEMENTAL INFORMATION

Supplemental Information includes one table and can be found with this article online at http://dx.doi.org/10.1016/j.ymthe.2017.03.037.

AUTHOR CONTRIBUTIONS

P.L. and D.E.S. conceived and coordinated this study; Y.M., J.A.W., and Y.N. designed and conducted in vivo experiments (enzyme replacement, toxicity, gait analysis) and biochemical analysis; J.A.W., D.E.S., and P.L., conducted and interpreted morphological studies of TPP1 uptake; D.F.M., D.E.S., and P.L. conducted statistical analyses; R.D. designed and conducted morphological experiments on uptake of fixable tracer and time course experiments on peptide and protein distribution; W.A.B. designed and conducted pharmacokinetic experiments utilizing radiolabeled tracers; Y.N. conducted in vitro cytotoxicity studies; K.R. conducted pathology analyses; and J.G. performed EEG experiments. The initial draft of the manuscript was written by Y.M., D.E.S. and P.L., while all authors contributed toward subsequent revisions prior to submission.

CONFLICTS OF INTEREST

P.L. and D.E.S. have received royalty payments as inventors on patent 8029781 ("Methods of Treating a Deficiency of Functional Tripeptidyl Peptidase I [CLN2] Protein"), which is licensed to BioMarin Pharmaceutical Inc. The other authors declare no conflicts of interest.

ACKNOWLEDGMENTS

We thank Dr. Wenjin Chen (Cancer Institute of New Jersey) for help with microscopy and Derek Kennedy and colleagues (Biomarin) for providing rhTPP1. We also thank Kristin Bullock (University of Washington) for performing pharmacokinetics studies, Benjamin McNeil and Xinzhong Dong (Johns Hopkins School of Medicine) for experiments involving *Mrgprb2*$^{-/-}$ mice, and Vijayalakshmi Santhakumar (Rutgers New Jersey Medical School) for EEG analysis. We also thank Dr. Gobinda Sarkar (Mayo Foundation) for sharing data prior to publication. This project was supported by NIH grant NS37918 (to P.L.). Mass spectrometry was conducted by the Biological Mass Spectrometry Facility of Robert Wood Johnson Medical School and Rutgers University, supported in part by NIH grants P30NS046593 and S10RR024584. Y.M. was supported by a grant from the Zhejiang Provincial Natural Science Foundation of China (LY16H080008) and by fellowships from the Batten Disease Support and Research Association and Cures Within Reach funded by Noah's Hope, Hope 4 Bridget, Fight for Nicolas, and Jasper Against Batten. This research was also supported by NIH grant P30CA072720 to the Rutgers Cancer Institute of New Jersey (to D.F.M. and the Imaging Shared Resource) and NIEHS Center grant P30ES005022.

REFERENCES

1. Schiffmann, R. (2010). Therapeutic approaches for neuronopathic lysosomal storage disorders. J. Inherit. Metab. Dis. *33*, 373–379.
2. Schultz, M.L., Tecedor, L., Chang, M., and Davidson, B.L. (2011). Clarifying lysosomal storage diseases. Trends Neurosci. *34*, 401–410.
3. Meng, Y., Sohar, I., Sleat, D.E., Richardson, J.R., Reuhl, K.R., Jenkins, R.B., Sarkar, G., and Lobel, P. (2014). Effective intravenous therapy for neurodegenerative disease with a therapeutic enzyme and a peptide that mediates delivery to the brain. Mol. Ther. *22*, 547–553.
4. Sleat, D.E., Wiseman, J.A., El-Banna, M., Kim, K.H., Mao, Q., Price, S., Macauley, S.L., Sidman, R.L., Shen, M.M., Zhao, Q., et al. (2004). A mouse model of classical late-infantile neuronal ceroid lipofuscinosis based on targeted disruption of the CLN2 gene results in a loss of tripeptidyl-peptidase I activity and progressive neurodegeneration. J. Neurosci. *24*, 9117–9126.
5. Sleat, D.E., Donnelly, R.J., Lackland, H., Liu, C.G., Sohar, I., Pullarkat, R.K., and Lobel, P. (1997). Association of mutations in a lysosomal protein with classical late-infantile neuronal ceroid lipofuscinosis. Science *277*, 1802–1805.
6. Xu, S., Wang, L., El-Banna, M., Sohar, I., Sleat, D.E., and Lobel, P. (2011). Large-volume intrathecal enzyme delivery increases survival of a mouse model of late infantile neuronal ceroid lipofuscinosis. Mol. Ther. *19*, 1842–1848.
7. Meng, Y., Sohar, I., Wang, L., Sleat, D.E., and Lobel, P. (2012). Systemic administration of tripeptidyl peptidase I in a mouse model of late infantile neuronal ceroid lipofuscinosis: effect of glycan modification. PLoS ONE *7*, e40509.
8. Sarkar, G., Curran, G.L., Mahlum, E., Decklever, T., Wengenack, T.M., Blahnik, A., Hoesley, B., Lowe, V.J., Poduslo, J.F., and Jenkins, R.B. (2011). A carrier for non-covalent delivery of functional beta-galactosidase and antibodies against amyloid plaques and IgM to the brain. PLoS ONE *6*, e28881.
9. Westergren, I., and Johansson, B.B. (1993). Altering the blood-brain barrier in the rat by intracarotid infusion of polycations: a comparison between protamine, poly-L-lysine and poly-L-arginine. Acta Physiol. Scand. *149*, 99–104.
10. Strausbaugh, L.J. (1987). Intracarotid infusions of protamine sulfate disrupt the blood-brain barrier of rabbits. Brain Res. *409*, 221–226.
11. Ballarín-González, B., and Howard, K.A. (2012). Polycation-based nanoparticle delivery of RNAi therapeutics: adverse effects and solutions. Adv. Drug Deliv. Rev. *64*, 1717–1729.
12. Godbey, W.T., Wu, K.K., and Mikos, A.G. (2001). Poly(ethylenimine)-mediated gene delivery affects endothelial cell function and viability. Biomaterials *22*, 471–480.
13. Moghimi, S.M., Symonds, P., Murray, J.C., Hunter, A.C., Debska, G., and Szewczyk, A. (2005). A two-stage poly(ethylenimine)-mediated cytotoxicity: implications for gene transfer/therapy. Mol. Ther. *11*, 990–995.
14. Chang, S.W., Westcott, J.Y., Henson, J.E., and Voelkel, N.F. (1987). Pulmonary vascular injury by polycations in perfused rat lungs. J. Appl. Physiol. (1985) *62*, 1932–1943.
15. Kircheis, R., and Wagner, E. (2004). Polymeric Gene Delivery: Principles and Applications (CRC Press).
16. Bolhassani, A., Jafarzade, B.S., and Mardani, G. (2017). In vitro and in vivo delivery of therapeutic proteins using cell penetrating peptides. Peptides *87*, 50–63.
17. Hervé, F., Ghinea, N., and Scherrmann, J.M. (2008). CNS delivery via adsorptive transcytosis. AAPS J. *10*, 455–472.
18. Wadia, J.S., Stan, R.V., and Dowdy, S.F. (2004). Transducible TAT-HA fusogenic peptide enhances escape of TAT-fusion proteins after lipid raft macropinocytosis. Nat. Med. *10*, 310–315.
19. Wiseman, J.A., Meng, Y., Nemtsova, Y., Matteson, P.G., Millonig, J.H., Moore, D.F., Sleat, D.E., and Lobel, P. (2017). Chronic enzyme replacement to the brain of a late infantile neuronal ceroid lipofuscinosis mouse has differential effects on phenotypes of disease. Mol. Ther. Methods Clin. Dev. *4*, 204–212.
20. Dohgu, S., Ryerse, J.S., Robinson, S.M., and Banks, W.A. (2012). Human immunodeficiency virus-1 uses the mannose-6-phosphate receptor to cross the blood-brain barrier. PLoS ONE *7*, e39565.
21. Urayama, A., Grubb, J.H., Sly, W.S., and Banks, W.A. (2004). Developmentally regulated mannose 6-phosphate receptor-mediated transport of a lysosomal enzyme across the blood-brain barrier. Proc. Natl. Acad. Sci. USA *101*, 12658–12663.
22. Urayama, A., Grubb, J.H., Banks, W.A., and Sly, W.S. (2007). Epinephrine enhances lysosomal enzyme delivery across the blood brain barrier by up-regulation of the mannose 6-phosphate receptor. Proc. Natl. Acad. Sci. USA *104*, 12873–12878.
23. Gutierrez, E.G., Banks, W.A., and Kastin, A.J. (1993). Murine tumor necrosis factor alpha is transported from blood to brain in the mouse. J. Neuroimmunol. *47*, 169–176.
24. Triguero, D., Buciak, J., and Pardridge, W.M. (1990). Capillary depletion method for quantification of blood-brain barrier transport of circulating peptides and plasma proteins. J. Neurochem. *54*, 1882–1888.

25. Croy, J.E., Brandon, T., and Komives, E.A. (2004). Two apolipoprotein E mimetic peptides, ApoE(130-149) and ApoE(141-155)2, bind to LRP1. Biochemistry *43*, 7328–7335.

26. Bechara, C., Pallerla, M., Zaltsman, Y., Burlina, F., Alves, I.D., Lequin, O., and Sagan, S. (2013). Tryptophan within basic peptide sequences triggers glycosaminoglycan-dependent endocytosis. FASEB J. *27*, 738–749.

27. McNeil, B.D., Pundir, P., Meeker, S., Han, L., Undem, B.J., Kulka, M., and Dong, X. (2015). Identification of a mast-cell-specific receptor crucial for pseudo-allergic drug reactions. Nature *519*, 237–241.

28. Sarkar, G., Curran, G.L., Sarkaria, J.N., Lowe, V.J., and Jenkins, R.B. (2014). Peptide carrier-mediated non-covalent delivery of unmodified cisplatin, methotrexate and other agents via intravenous route to the brain. PLoS ONE *9*, e97655.

29. Broadwell, R.D., and Balin, B.J. (1985). Endocytic and exocytic pathways of the neuronal secretory process and trans-synaptic transfer of wheat germ agglutinin-horseradish peroxidase in vivo. J. Comp. Neurol. *242*, 632–650.

30. Villegas, J.C., and Broadwell, R.D. (1993). Transcytosis of protein through the mammalian cerebral epithelium and endothelium. II. Adsorptive transcytosis of WGA-HRP and the blood-brain and brain-blood barriers. J. Neurocytol. *22*, 67–80.

31. Banks, W.A., and Broadwell, R.D. (1994). Blood to brain and brain to blood passage of native horseradish peroxidase, wheat germ agglutinin, and albumin: pharmacokinetic and morphological assessments. J. Neurochem. *62*, 2404–2419.

32. Christianson, H.C., and Belting, M. (2014). Heparan sulfate proteoglycan as a cell-surface endocytosis receptor. Matrix Biol. *35*, 51–55.

33. Sleat, D.E., El-Banna, M., Sohar, I., Kim, K.H., Dobrenis, K., Walkley, S.U., and Lobel, P. (2008). Residual levels of tripeptidyl-peptidase I activity dramatically ameliorate disease in late-infantile neuronal ceroid lipofuscinosis. Mol. Genet. Metab. *94*, 222–233.

34. Daneman, R., Zhou, L., Kebede, A.A., and Barres, B.A. (2010). Pericytes are required for blood-brain barrier integrity during embryogenesis. Nature *468*, 562–566.

35. Banks, W.A., Kastin, A.J., Komaki, G., and Arimura, A. (1993). Passage of pituitary adenylate cyclase activating polypeptide1-27 and pituitary adenylate cyclase activating polypeptide1-38 across the blood-brain barrier. J. Pharmacol. Exp. Ther. *267*, 690–696.

36. Banks, W.A., Kastin, A.J., Huang, W., Jaspan, J.B., and Maness, L.M. (1996). Leptin enters the brain by a saturable system independent of insulin. Peptides *17*, 305–311.

37. Pettit, W.A., DeLand, F.H., Bennett, S.J., and Goldenberg, D.M. (1980). Improved protein labeling by stannous tartrate reduction of pertechnetate. J. Nucl. Med. *21*, 59–62.

38. Blasberg, R.G., Fenstermacher, J.D., and Patlak, C.S. (1983). Transport of alpha-aminoisobutyric acid across brain capillary and cellular membranes. J. Cereb. Blood Flow Metab. *3*, 8–32.

39. Patlak, C.S., Blasberg, R.G., and Fenstermacher, J.D. (1983). Graphical evaluation of blood-to-brain transfer constants from multiple-time uptake data. J. Cereb. Blood Flow Metab. *3*, 1–7.

40. R Core Team (2015). R: a language and environment for statistical computing. www.R-project.org/.

41. Yu, J., Proddutur, A., Swietek, B., Elgammal, F.S., and Santhakumar, V. (2016). Functional reduction in cannabinoid-sensitive heterotypic inhibition of dentate basket cells in epilepsy: impact on network rhythms. Cereb. Cortex *26*, 4299–4314.

42. Sleat, D.E., Della Valle, M.C., Zheng, H., Moore, D.F., and Lobel, P. (2008). The mannose 6-phosphate glycoprotein proteome. J. Proteome Res. *7*, 3010–3021.

43. Craig, R., Cortens, J.P., and Beavis, R.C. (2004). Open source system for analyzing, validating, and storing protein identification data. J. Proteome Res. *3*, 1234–1242.

44. Liu, H., Sadygov, R.G., and Yates, J.R., 3rd (2004). A model for random sampling and estimation of relative protein abundance in shotgun proteomics. Anal. Chem. *76*, 4193–4201.